Cell

Nanoscale Organization of Hedgehog Is Essential for Long-Range Signaling

Neha Vyas,[1,2] Debanjan Goswami,[1] A. Manonmani,[1,4] Pranav Sharma,[1,5] H.A. Ranganath,[2,6] K. VijayRaghavan,[1] L.S. Shashidhara,[3] R. Sowdhamini,[1] and Satyajit Mayor[1,*]
[1]National Centre for Biological Sciences, Tata Institute of Fundamental Research, Bellary Road, Bangalore 560 065, India
[2]Department of Studies in Zoology, University of Mysore, Mysore 570 006, India
[3]Centre for Cellular and Molecular Biology, Uppal Road, Hyderabad 500 007, India
[4]Present address: Max Planck Institute of Molecular Cell Biology and Genetics, Pfotenhauerstr 108, 01307 Dresden, Germany
[5]Present address: Cold Spring Harbor Laboratory, Cold Spring Harbor, New York 11724, USA
[6]Present address: Vice Chancellor's Office, Bangalore University, Bangalore 560 001, India
*Correspondence: mayor@ncbs.res.in
DOI 10.1016/j.cell.2008.05.026

SUMMARY

Hedgehog (Hh) plays crucial roles in tissue-patterning and activates signaling in Patched (Ptc)-expressing cells. Paracrine signaling requires release and transport over many cell diameters away by a process that requires interaction with heparan sulfate proteoglycans (HSPGs). Here, we examine the organization of functional, fluorescently tagged variants in living cells by using optical imaging, FRET microscopy, and mutational studies guided by bioinformatics prediction. We find that cell-surface Hh forms suboptical oligomers, further concentrated in visible clusters colocalized with HSPGs. Mutation of a conserved Lys in a predicted Hh-protomer interaction interface results in an autocrine signaling-competent Hh isoform—incapable of forming dense nanoscale oligomers, interacting with HSPGs, or paracrine signaling. Thus, Hh exhibits a hierarchical organization from the nanoscale to visible clusters with distinct functions.

INTRODUCTION

Hedgehog (Hh) is involved in cell-fate specification and tissue patterning during animal development by activation of distinct target genes in a concentration-dependent manner. The mechanisms by which gradients of such morphogens are established have been the focus of much investigation (Ashe and Briscoe, 2006) and are expected to result as a consequence of the amount released, rate of capture and endocytosis in the receiving cell, and transport across developing tissues (Tabata and Takei, 2004).

Hh is synthesized as a 45 KDa precursor protein whose C-terminal domain (~25 KDa) is autocatalytically cleaved and degraded (Porter et al., 1995), whereas the remaining 20 KDa N-terminal domain is covalently modified by cholesterol at the C terminus and palmitoylated at the N-terminus (Pepinsky et al., 1998; Porter et al., 1996). Binding of Hh to its receptor Patched (Ptc) activates a signaling cascade via molecules such as Smo and Ci. Typically, Hh-producing cells do not activate signaling because they lack Ci, making the release and transport of this molecule mandatory.

Although the mechanisms that control the release of Hh are poorly understood, heparan sulfate proteoglycans (HSPGs) and lipoprotein particles have been implicated in its transport. In *Drosophila*, a class of HSPGs, glypicans (Dally and Dally-like proteins [Dlp]), have been implicated in transport of different morphogens, including Hh (Lin, 2004). Several studies have shown that HSPGs are required for the movement of Hh across cell layers in wing discs (Bellaiche et al., 1998; Callejo et al., 2006; Han et al., 2004). Cells mutant for HSPGs and wild-type cells in the "shadow" of mutant clones fail to receive Hh (Callejo et al., 2006; Han et al., 2004). Also implicated in the movement of Hh across developing tissue are lipoprotein particles (Panakova et al., 2005), containing Dally and Dlp (Eugster et al., 2007).

Lipid modification of Hh, in particular its cholesterol moiety, have been well studied (Mann and Beachy, 2004). It is proposed to function as an anchor for Hh in the plasma membrane and aids in restricting the range of Hh signaling (Mann and Beachy, 2004), whereas palmitoylation seems to be required for Hh signaling (Chamoun et al., 2001).

The roles of the lipid modifications in Hh organization have also been explored. It has been shown that heterologously tagged isoforms of Sonic Hedgehog (Shh) can be coimmunoprecipitated, suggesting that Shh can form homomultimers (Zeng et al., 2001). Further, gel filtration assays have suggested that Hh and Shh can form high molecular weight complexes ranging up to 4000 KDa (Chen et al., 2004; Gallet et al., 2006; Zeng et al., 2001). These high molecular weight complexes are not observed in the absence of cholesterol or palmitoyl modification, suggesting that the multimerization of Hh/Shh requires the presence of these lipid anchors (Chen et al., 2004; Zeng et al., 2001). Hh has also been visualized in cholesterol anchor-dependent, large punctate structures (LPS) by immunofluorescence microscopy (Gallet et al., 2003; Porter et al., 1996). Although Hh forms multimers of varied sizes, the relationship of the LPS and the higher molecular weight complexes remains ambiguous. In this

background, examination of the organization of Hh in live cells, under physiologically relevant conditions, with high-resolution imaging will be vital to accurately relate predictions made from biochemical and other experiments to specific cellular functions.

In this paper, we examine the cell-surface organization of Hh in living cells and its developmental consequence by using intrinsically fluorescent and functional isoforms of Hh (Hh-GFP and Hh-mCFP). Our data suggest that interplay of organization at different length scales is required for efficient Hh transport, a critical cue for which is localized in the protein itself. This protein-based nanoscale organization is required for efficient interaction of Hh with cell-surface HSPGs, formation of larger-scale clusters, and efficient transport of Hh across cell layers. Mutant isoforms that do not form protein-dependent nanoscale clusters are incapable of binding HSPGs and cannot be transported over multiple cell diameters, but remain signaling competent in autologous membranes and to adjacent cells.

RESULTS

GFP- and mCFP-Tagged Hh Variants Are Signaling Competent and Functional during Development

We designed a *hh-gfp* fusion gene (Figure 1A) to examine Hh organization in live cells and transgenic animals by using the GAL4 and UAS system (Phelps and Brand, 1998). We tested this fusion construct in several ways, to ensure that the encoded Hh-GFP fusion protein functioned similarly to wild-type Hh. First, UAS-Hh-GFP was driven in flies by the vestigial wing-margin driver (*vg*-GAL4). The resulting ectopic wing-blade patterns (Figure 1B) were similar to those observed upon UAS-Hh expression (Figure 1C). Second, when Hh-GFP is expressed in the peripodial membrane (PM) of the wing disc with the *ultrabithorax* (*Ubx*)-GAL4 driver, *decapentaplegic* (*dpp*), a target of Hh signaling, is expressed ectopically in the entire anterior compartment, as indicated by a *dpp*-lacZ reporter (Figure 1D). This is similar to that seen upon Hh expression with the same GAL4 driver (Pallavi and Shashidhara, 2005). Hh-GFP and Hh also show identical signaling range and efficiency when expressed in flp-out clones in the anterior domain of wing discs with respect to the activation of Ptc (Figure 1E and Figures S1D–S1I available online). Finally, the lethality of a temperature-sensitive mutant, hh^{ts2}, can be completely rescued by the expression of Hh-GFP or Hh under the control of an *engrailed* (*en*)-GAL4 driver (Figure 1F).

We also generated a Hh-mCFP protein by inserting sequences encoding mCFP at the same location in the *hh* as was done to generate the GFP fusion. We similarly tested the function of this fusion protein in flies, first by using the *vg*-GAL4 driver (data not shown) and next by using the *Ubx*-GAL4 driver as done above for the Hh-GFP protein (Figures S1A–S1C and Figure 1D). Identical results were obtained.

Fluorescently Tagged Hh Exhibits Diffuse and Clustered Distributions at the Cell Surface

We used Hh-GFP and Hh-mCFP fusion to explore the organization of Hh in cell membranes in vivo and in tissue culture. Hh-GFP was expressed in the PM with the *Ubx*-GAL4 driver, and its cell-surface organization was examined with fluorescently labeled Fab fragments of antibodies against GFP. The use of labeled Fab fragments prevents artifacts generated by clustering of the lipid-anchored proteins caused by secondary antibody-induced crosslinking (Mayor and Maxfield, 1995). In addition, tissue samples were labeled on ice, in a nonpermeabilized condition, to prevent labeling of intracellular compartments. Hh-GFP is observed in a diffuse distribution with a significant fraction as optically resolvable clusters (visible clusters) at the cell surface (Figures 2A and 2B).

We next examined whether such a distribution is also seen in S2R+ cells, in which cell-surface distributions of GFP-labeled molecules can be examined at higher resolution because of the absence of scattering (intrinsic to the thicker tissue samples taken from the animal): A similar cell-surface distribution—both in terms of a diffuse distribution and visible clusters—is seen (Figures 2C and 2D); ~60% of Hh-GFP fluorescence is present in a clustered distribution in these cells (Figure S2A). A similar distribution is also observed when UAS-Hh is expressed in S2R+ cells (Figure 2E). These results show that the surface distribution of Hh-GFP seen in a functional context is very similar to that observed in S2R+ cells. Although we discuss the significance of this visible organization later, these results allow us to examine, in S2R+ cells, the basis for this visible organization.

A possible concern regarding Hh-GFP, even in a context where the fusion protein is functional, is that the surface organization may not necessarily reflect that of the native protein but could be a consequence of the GFP label, particularly since GFP might dimerize (Zhang et al., 2002). We therefore examined surface organization of the Hh-mCFP fusion protein (Figure 3A); this isoform is organized identical to Hh-GFP (Figures 2C, 2D, 3B, and 3C and Figure S2A). Thus, mCFP and GFP fusion proteins exhibit identical properties in assays of both function and surface organization to untagged Hh, thereby also allowing us to use these constructs interchangeably in our experiments.

Clustering of Hh at the Cell Surface Requires the N-Terminal Signaling Domain

Since lipid modifications have been proposed to be responsible for clustering (Chen et al., 2004; Gallet et al., 2003), we examined whether they were sufficient for the formation of visible clusters at the cell surface. We generated a construct where a major portion of the Hh polypeptide (residues 115–255) was deleted (HhΔ140-mCFP; Figure 3A′). This variant of Hh retains regions required for cholesterol and palmitoyl modification but lacks the entire N-terminal domain. We observed that HhΔ140-mCFP fails to make visible clusters at the cell surface in S2R+ cells (Figures 3D and 3E), although it is expressed at similar surface levels as fluorescently tagged Hh isoforms (Figure S2B). The fraction of fluorescence intensity present in optically resolvable clusters is no different from that measured for the diffusely distributed GFP-tagged GPI-anchored protein (GFP-GPI; Figure S2A). This suggests that the lipid modifications alone are not sufficient for organizing Hh into visible clusters; instead, the Hh signaling domain is necessary for this organization.

Another possibility is that the visible clusters could be generated by interactions with molecules such as the multimeric Hh receptor, Ptc (Lu et al., 2006). S2R+ cells do express Ptc, albeit at very low levels (Lum et al., 2003). Nevertheless, we further lowered the levels of *ptc* expression by RNA interference (RNAi) in

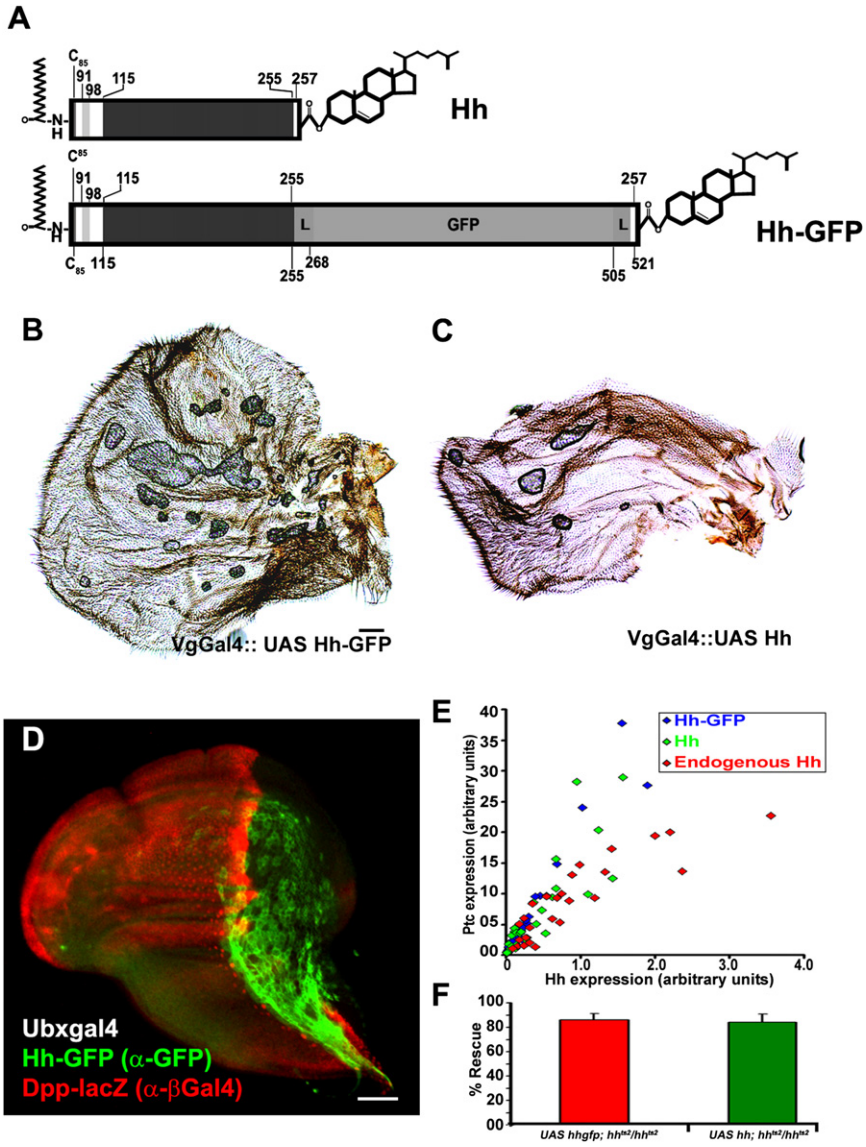

Figure 1. Hh-GFP Is a Functional Homolog of Hh

(A) Posttranslational modifications of Hh and Hh-GFP where the GFP coding sequence has been inserted at position 255 adjacent to the conserved GCF triad. In the mature Hh, Gly257 is covalently modified with cholesterol after cleavage of the autocatalytic C-terminal domain. Hh is palmitoylated at the N terminus at Cys85.

(B and C) Expression of either Hh-GFP (B) or Hh (C) along the dorsoventral boundary of wing discs with *vg*-GAL4 gives rise to similarly mispatterned adult wings.

(D) Wing disc ectopically expressing Hh-GFP (green) in PM cells with the *Ubx*-GAL4 driver. *dpp*-lacZ (red) is activated in entire anterior domain of wing disc.

(E) Graph representing signaling efficiency of UAS Hh (green), UAS Hh-GFP (blue), and endogenous Hh (in red). Levels of Ptc activation by UAS Hh, UAS Hh-GFP, and endogenous Hh are plotted against their expression levels. Endogenous Hh (in posterior domain) and Ptc levels (along AP boundary) are scored from the same discs expressing UAS Hh flp-out clones. All images were acquired with identical parameters. Data are obtained from 25–35 flp-out clones in wing disc generated with *actin5C*>*CD2*>GAL4 as described in the Supplemental Experimental Procedures, and stained for surface pool of Hh isoforms with anti-Hh antibodies.

(F) Expression of UAS-Hh-GFP or UAS-Hh with the *en*-GAL4 driver result in the rescue of the lethality of hh^{ts2} homozygous flies grown at the restrictive temperature. Bars represent the mean + SD from three different experiments, of the percentage of adults that emerge. Indicated transgenic flies were grown at the restrictive temperature, with at least 80 flies examined in each genotype.

Scale bars represent 40 μm in (B) and (C) and 20 μm in (D).

S2R+ cells and examined the effect on surface organization. Although Ptc was completely downregulated in RNAi-treated S2R+ cells (Figure S3D), the surface distribution of Hh-GFP in these cells remained undisturbed (Figures S3A–S3C). These results confirm that Ptc is not involved in visible clustering of Hh at the cell surface and suggest that the clustering potential of Hh lies in its signaling domain.

HSPGs Are Involved in Forming Visible Clusters of Hh

HSPGs play an important role in the mechanism of transport of Hh across cells (Lin, 2004); therefore, we reasoned that HSPGs may be involved in cell-surface organization of Hh. We first examined if the visible clusters containing Hh fusion protein colocalized with Dlp, an endogenously expressed HSPG in S2R+ cells (DasGupta et al., 2005). Immunostaining with antibodies against Dlp showed that the visible clusters of Hh-mCFP completely colocalize with Dlp (Figures 4A–4C). Interestingly, Dlp shows a clustered organization even in untransfected cells, suggesting that Dlp may be intrinsically clustered (Figure 4E).

Experiments with Shh suggest the involvement of conserved positively charged residues, the Cardin Weintraub sequence (CW), in mediating interactions with negatively charged HSPGs (Rubin et al., 2002). We generated a Hh isoform that lacks this region (HhΔCW-mCFP; Figure 4D). HhΔCW-mCFP when expressed in S2R+ cells showed a completely diffuse distribution (Figures 4F and 4G), despite the clustered distribution of endogenous Dlp (Figure 4H). As observed with HhΔ140-mCFP, the fraction of fluorescence intensity of HhΔCW-mCFP present in optically resolvable clusters is not very different from that measured for the diffusely distributed GFP-GPI protein (Figure S2A). Conversely, when we used a combination of RNAis to deplete multiple HSPG-containing proteins in S2R+ cells (Figure 4N), Hh-mCFP failed to form visible clusters (Figures 4L and 4M and Figure S2A). Taken together, these data show that

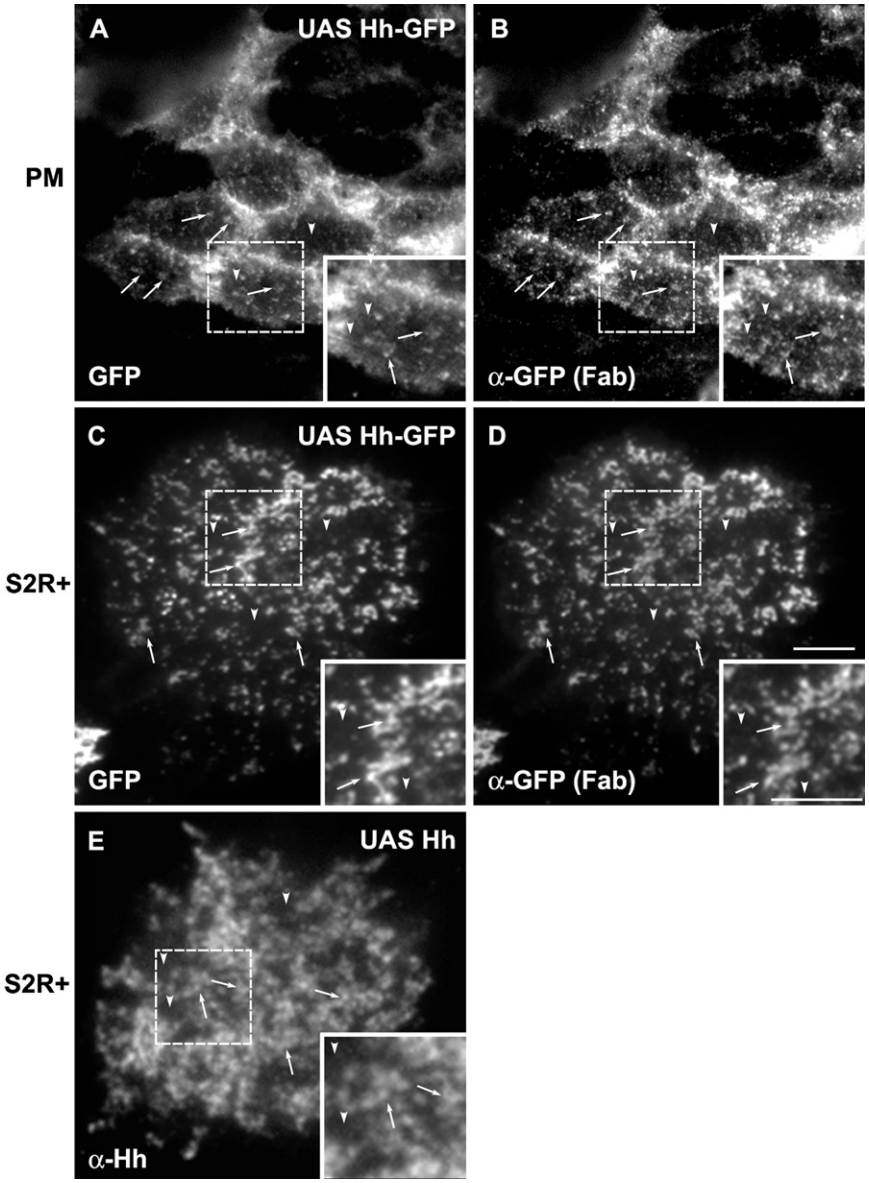

Figure 2. Hh-GFP Exhibits Visibly Clustered as well as Diffuse Distribution at the Cell Surface

(A and B) Distribution of Hh-GFP expressed in PM cells of the wing disc with the *Ubx*-GAL4 driver observed by examining the fluorescence of GFP (A) or that of the extracellular pool of Hh-GFP, marked by Cy3-labeled anti-GFP (Cy3α-GFP) Fab fragments (B). Note that in both cases, Hh-GFP is present as diffuse (arrow head) and visibly clustered (arrows) distribution at the cell surface.

(C–E) S2R+ cells were transfected with *actin*-GAL4 along with UAS-Hh-GFP (C and D) or UAS-Hh (E) and labeled at the cell surface with Cy3α-GFP Fab fragments (D) or anti-Hh antibodies followed by labeled secondary antibodies (E) and imaged with a wide-field microscope. Note that both Hh-GFP and Hh exhibit diffuse (arrowheads) and visibly clustered (arrows) distribution at the cell surface. Insets show a magnified view of the region marked by the square. Scale bars represent 5 μm.

the CW motif is necessary for the formation of visible clusters of Hh that colocalize with HSPG-containing proteins such as Dlp. However, the lack of a visibly clustered distribution of HhΔ140-mCFP (Figures 3D, 3E, and 4I–4K) that contains the CW motif (Figure 3A′) suggests that this motif on its own is not sufficient for the generation of these clusters.

Hh Forms Nanoscale Oligomers, Enriched in the Visible Clusters

To further explore the basis for the formation of visible clusters of Hh, we examined the organization of this protein at the nanometer scale by using a variation of Forster's resonance energy transfer, namely, homo-FRET (Altman et al., 2007; Sharma et al., 2004; Varma and Mayor, 1998). FRET measures interfluorophore distances at the 1–10 nm range (Rao and Mayor, 2005). Measurement of fluorescence emission anisotropy upon excitation with polarized excitation is a very sensitive indicator of FRET between GFP fluorophores (Rao and Mayor, 2005). Homo-FRET efficiencies may be obtained by performing a time-resolved anisotropy (TRA) decay experiment. Here, the rate of decay of anisotropy of emission generated by a pulse of multiphoton excitation in a confocal volume is monitored by time-correlated single-photon counting (Altman et al., 2007).

The anisotropy decay profile for the GFP or mCFP fluorophores undergoing homo-FRET typically gives rise to two decay components (Figure S4B): A slow-decay component in the tens of nanoseconds time scale reports on the rotation of the protein-embedded fluorophore, and a fast-decay component on the subnanosecond time scale reports on homo-FRET between GFP or mCFP monomers (Altman et al., 2007; Gautier et al., 2001). The fast rate of decay is a direct indicator of the rate of energy transfer and therefore provides a sensitive measure of the proximity between fluorophores; a faster rate indicates greater proximity, and vice versa (Gautier et al., 2001; Sharma et al., 2004). Anisotropy decay rates may be extracted from the empirical anisotropy data by appropriate fitting routines and procedures described in detail previously (Altman et al., 2007) (Figures S4C and S4D).

We examined TRA decays in both the diffuse and visibly clustered regions on the surface of S2R+ cells expressing Hh-mCFP (Figure 5A) or Hh-GFP (Figure S5C). A fast-decay component indicative of FRET is characteristic of both regions (Figure 5A, right panel). Although the fast-decay rates in both regions are similar (Table 1; $p > 0.5$; Figure S9), the amplitude of the fast-decay

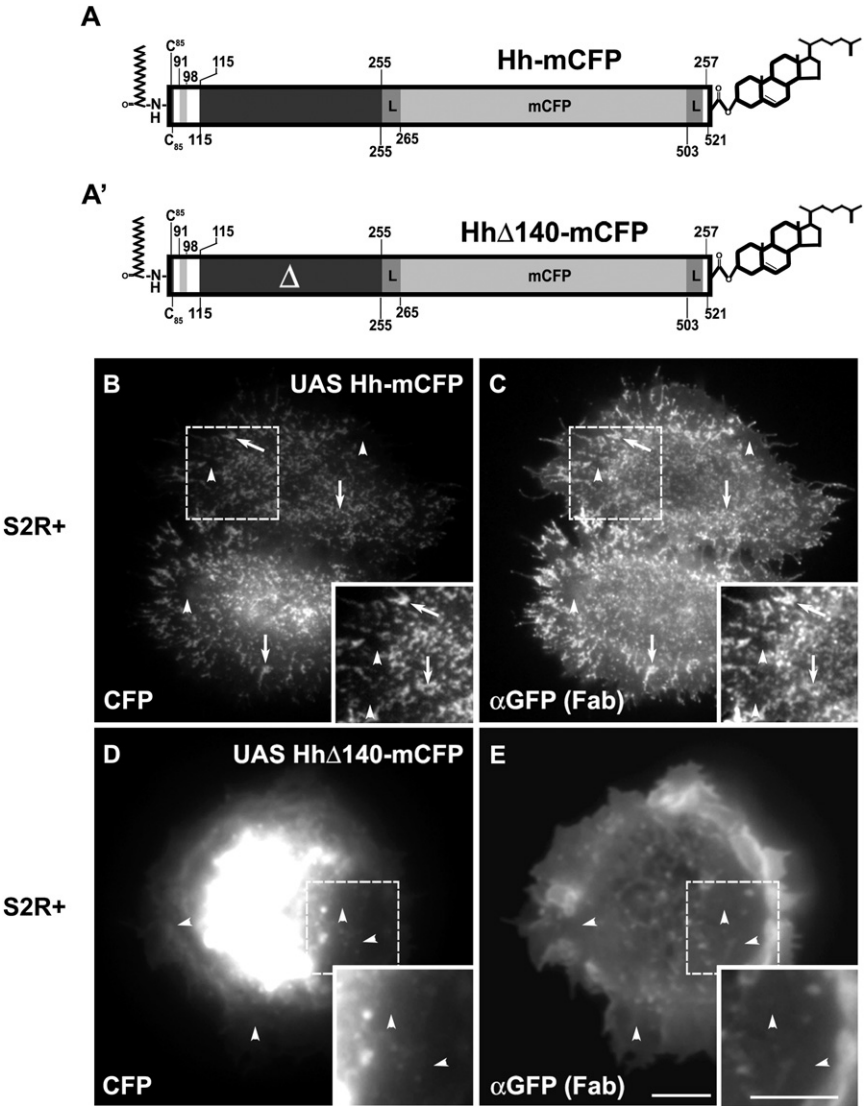

Figure 3. Formation of Visible Clusters Requires Hh Signaling Domain

(A) Cartoon depicts posttranslational modifications of Hh-mCFP with mCFP coding sequence inserted in the Hh sequence at the same position as GFP described in Figure 1A.

(A′) Depicts a deletion mutant of Hh-mCFP, HhΔ140-mCFP, wherein residues 115 to 255 have been deleted from the sequence encoding Hh-mCFP.

(B–E) S2R+ cells were transfected with *actin*-GAL4 along with UAS-Hh-mCFP (B and C) or UAS-HhΔ140-mCFP (D and E) and labeled at the cell surface with Cy3α-GFP (C and E) and imaged with a wide-field microscope. Note that although Hh-mCFP exhibits diffuse (arrowheads) and visibly clustered (arrows) distribution at the cell surface, the distribution of HhΔ140-mCFP is diffuse (arrowheads). Insets show a magnified view of the region marked by the square. Scale bars represent 5 μm.

component is significantly higher in the visible regions (Table 1; $p < 0.01$; Figures S4E and S4F). This implies that similarly arranged nanoscale oligomers of Hh-mCFP undergoing homo-FRET are present in both regions; however, in the visible clusters, the population of these oligomers is higher. It should be noted that at similar fluorophore concentration in the membrane, the molecules are to far apart that FRET is extremely unlikely in the absence a specific clustering mechanism (Sharma et al., 2004). These results indicate that Hh-mCFP forms optically unresolved nanoscale oligomers at the cell surface, which are further enriched in the visible clusters at cell surface. Similar anisotropy decay profiles of Hh-GFP in the diffuse and visible cluster regions are observed in S2R+ cells (Figure S5C; Table 1), confirming the ubiquitous nature of this level of organization of Hh. For comparison, we have juxtaposed anisotropy decay profiles for the well characterized GFP-GPI in membranes of mammalian cells, with the same molecule expressed in S2R+ cells and with Hh-GFP from the diffuse regions (Figures S5A and S5B).

The data also show that the nanoscale organization of Hh in the diffuse regions is different from the diffusely distributed GFP-GPI. Anisotropy decay rates (τ_{R1}; Table 1) for Hh-GFP and Hh-mCFP compared to GFP-GPI or GPI-anchored mCFP (mCFP-GPI; $p < 0.0001$), respectively, suggest that Hh forms denser (more compact) clusters than do GPI-anchored proteins (GPI-APs).

We next compared the anisotropy decay profiles of CFP in the diffusely distributed HhΔCW-mCFP (Figure 5B) and Hh-mCFP expressed in S2R+ cells depleted of HSPG-containing proteins by using multiple RNAi (DDPS; Figure 5C). Depletion of HSPG-containing proteins did not alter the fast anisotropy decay rate of Hh-mCFP (Table 1; $p > 0.5$). In addition, deletion of the ΔCW domain resulted in only a minor and statistically insignificant increase in the decay rate of the fast component (Table 1; $p \sim 0.02$). This is consistent with the presence of similar nanoscale oligomers in Hh-mCFP, HhΔCW-mCFP (Figure 5B), as well as in Hh-mCFP expressed in S2R+ cells treated with DDPS RNAi (Figure 5C and Figure S9). Further, the fraction of molecules undergoing FRET was also similar to that obtained for Hh-mCFP in the diffuse regions (Table 1). These results suggest that the nanoscale oligomers of Hh are formed independent of the ability to interact with cell-surface HSPGs.

Electrostatic Interaction between Hh Molecules Is Responsible for the Nanoscale Organization

Together, the results described above support the hypothesis that although interaction with HSPGs is necessary for formation of visible clusters of Hh, they are not required for nanoscale Hh organization. These results suggest that a region of the mature Hh polypeptide could be responsible for nanoscale oligomer

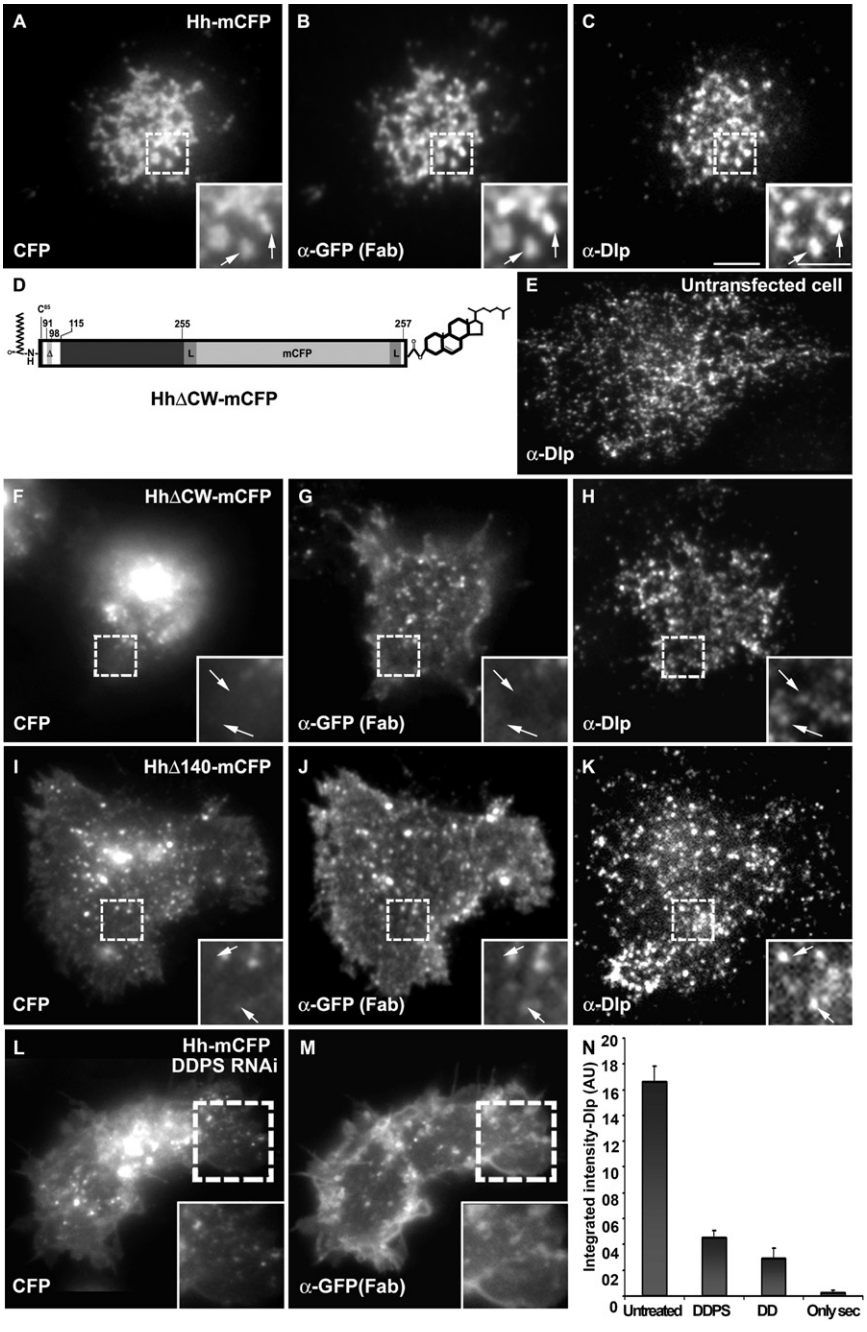

Figure 4. Cell-Surface HSPGs Are Colocalized with Visible Clusters of Hh

(A–C) S2R+ cells were transfected with *actin*-GAL4 along with UAS-Hh-mCFP (A), labeled at the cell surface with Cy5α-GFP Fab fragments (B) and anti-Dlp antibodies, and imaged after staining with a Fc-specific secondary antibody against anti-Dlp (C). Note visible clusters of Hh at the cell surface colocalize with endogenous Dlp clusters (arrows).

(D) Cartoon depicts a deletion mutant of Hh-mCFP, HhΔCW-mCFP, wherein residues 91 to 98 encoding the HSPG interacting domain have been deleted.

(E) Untransfected S2R+ cell stained for endogenous Dlp with anti-Dlp antibodies also show a clustered distribution.

(F–K) S2R+ cells were transfected with *actin*-GAL4 along with HhΔCW-mCFP (F–H) or HhΔ140-mCFP (I–K) were labeled at the cell surface with Cy5α-GFP Fab fragments (G and J) and anti-Dlp (H and K) antibodies and imaged after staining with a secondary antibody. Note that although endogenous Dlp is present in clusters (arrows), the surface distribution of HhΔCW-mCFP (G), or HhΔ140-mCFP (J) is diffuse.

(L and M) S2R+ cells depleted for endogenous HSPGs were transfected with *actin*-GAL4 and UAS Hh-mCFP (L) and labeled at cell surface with Cy5α-GFP Fab fragements (M).

(N) Graph represents integrated levels of endogenous Dlp quantitated in cells treated with RNAi to Dally, Dlp, Perlecan, and Syndecan (DDPS), Dally and Dlp (DD), and untreated cells, represented as mean ± SD. Experiment was repeated three times with similar results. Insets show a magnified view of the region marked by the square. Scale bars represent 5 μm, and 2.5 μm in the inset.

formation. To examine this possibility, we monitored the nanoscale organization of HhΔ140-mCFP (Figure 3A′). Anisotropy decay profiles obtained from HhΔ140-mCFP show that there is a detectable difference in decay rates and amplitude of the fast component, when compared to Hh-mCFP present in the diffuse regions (Figure 5D; Table 1). The fast component has a significantly slower decay rate ($p < 0.01$; Figure S9), indicating a looser interaction between the tagged molecules. Anisotropy decay parameters measured for the HhΔ140-mCFP construct mirror those obtained for a GPI also expressed in the same cells ($p \sim 0.5$; Figures S6A and S9; Table 1). These results suggest that sequences present in the N-terminal signaling domain of Hh are capable of forming nanoscale oligomers of Hh-mCFP more densely packed than HhΔ140-mCFP or mCFP-GPI.

To narrow the region in the mature protein which could mediate Hh-Hh interactions to organize molecules at the nanoscale, we used a predictive protein-docking software, Global Range Molecular Matching (GRAMM) to generate possible models for Hh-Hh interaction. One of the several models (data not shown for others) generated by GRAMM docking suggested interaction between Hh molecules where the putative interaction surface of one of the Hh protomers is predominantly electrostatic (Figures S7A and S7B). According to this model, Lys at position 132 is within electrostatic interaction distance of a negatively charged group of residues like Glu176, Asp214, and Glu227 (Figures S7A and S7B). In parallel, we also examined packing interactions in the crystal structure of Shh (Hall et al., 1995). We found similar electrostatic

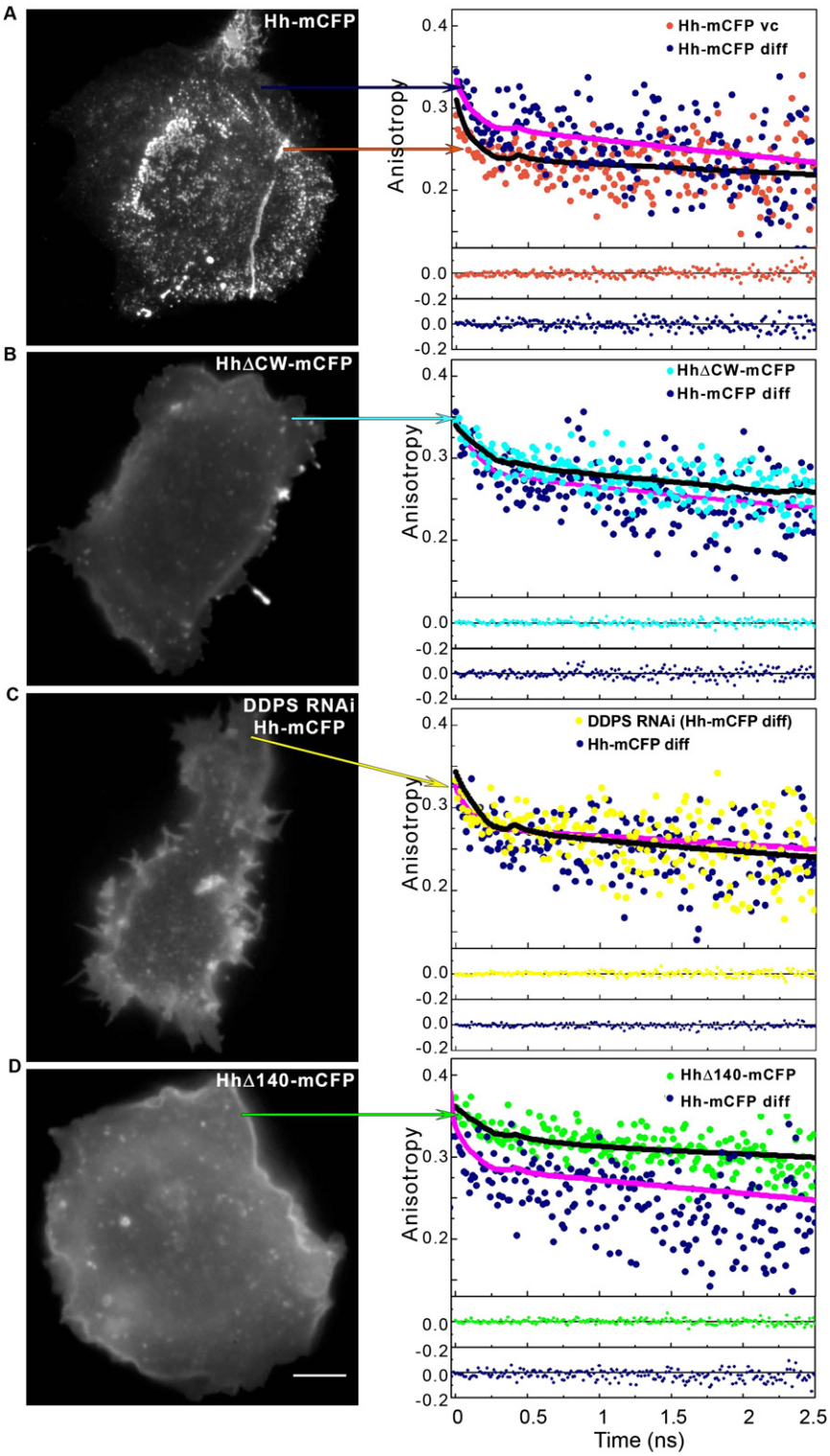

Figure 5. Anisotropy Decay Profiles of Hh-mCFP Detect Nanoscale Proximity between Hh Variants

S2R+ cells were transfected with *actin*-GAL4 along with UAS-Hh-mCFP (A), -HhΔCW-mCFP (B), -Hh-mCFP in DDPS RNAi-treated cells (C), or -HhΔ140-mCFP (D) and imaged after the cell-surface pool of the respective proteins was marked with fluorescently labeled anti-GFP Fab fragments with wide-field microscopy (left panels). Subsequently, a femtosecond pulsed laser was parked at selected positions at the cell surface, and time-resolved anisotropy decay profiles were collected from a confocal volume generated by multiphoton excitation, with a dual-channel TCSPC detection system. Anisotropy decays profiles (right panels) are obtained from single confocal volumes over indicated regions of the cell and fit as described in the Experimental Procedures. Note anisotropy decay profiles from diffuse regions of cells expressing Hh-mCFP (Hh-mCFP diff; blue circles in [A]–[D], right panels) exhibit a fast decay rate (<0.2 ns) comparable to those obtained from visible clusters (Hh-mCFP vc; orange circles in [A]), diffuse regions of DDPS RNAi-treated cells expressing Hh-mCFP (Hh-mCFP diff; yellow circles in [C]), or from cells expressing the diffusely distributed HhΔCW-mCFP (cyan circle in [B]); whereas the anisotropy decay rates from cells expressing HhΔ140-mCFP (green circles in D) are detectably slower (see also Table 1). The amplitude of the fast decay component is higher in regions containing visible clusters. The anisotropy decay profile of each Hh variant is plotted along with Hh-mCFP diff from the same experiment. All decays were fit to a biexponential model, and the residuals for the fit are plotted below. The pink line in all graphs indicates the fit for data points in blue, and the black line for orange, cyan, or green. The scale bar represents 5 μm.

interactions between Shh molecules (Figure 6A) involving an Arg residue (position 73). This residue, present in all homologous vertebrate Hh isoforms, represents a conservative substitution for Lys at position 132 that appears in all the different *Drosophila* Hh sequences (Figure S7C). Since analyses by both GRAMM (Hh) and the crystal structure (Shh) implicated a role for a positively charged residue at position 132 (Figures 6A–6C), we mutated this Lys 132 to Asp in Hh-mCFP (HhK132D-mCFP) to assess whether the nanoscale interaction between Hh molecules was affected. To ascertain that the protein products contain appropriate lipid modifications, we assessed their ability to partition into the detergent phase of Triton X-114 in a biochemical assay previously shown to detect lipid modifications of Hh (Porter et al., 1996). Hh-GFP, Hh-mCFP, and HhK132D-mCFP all partitioned into the detergent phase similar to the wild-type Hh protein, consistent with the presence of appropriate lipid modifications (Figure S11).

TRA measurements on S2R+-expressing HhK132D-mCFP showed a significant reduction ($p < 0.001$) in the efficiency of

Table 1. Anisotropy Decay Parameters of Hh-GFP and mCFP Variants

Constructs (n)	$r_0 \pm SD$	$\tau_{R1} \pm SD$ ($A_{R1} \pm SD$)	$\tau_{R2} \pm SD$ ($A_{R2} \pm SD$)	$r_{ss} \pm SD$
GFP-GPI CHO (5)	0.44 ± 0.01	0.284 ± 0.009 (0.075 ± 0.005)	35.2 ± 0.5 (0.698 ± 0.041)	0.380 ± 0.006
GFP-GPI (5) Cholesterol depleted[a]	0.42 ± 0.01	28.1 ± 4.1	NA	0.380 ± 0.02
GFP-GPI SR^+ (5)	0.44 ± 0.01	0.316 ± 0.048 (0.043 ± 0.009)	27.8 ± 2.2 (0.957 ± 0.009)	0.388 ± 0.008
Hh-GFP diff (5)	0.37 ± 0.01	0.087 ± 0.011 (0.093 ± 0.016)	38.5 ± 11.4 (0.907 ± 0.016)	0.317 ± 0.010
Hh-GFP vc (4)	0.37 ± 0.01	0.079 ± 0.025 (0.244 ± 0.103)	160.4 ± 19.2 (0.756 ± 0.103)	0.277 ± 0.035
mCFP-GPI (8)	0.41 ± 0.02	0.27 ± 0.01 (0.1 ± 0.02)	24.2 ± 1.3 (0.9 ± 0.02)	0.34 ± 0.01
Hh-mCFP diff (11)	0. 419 ± 0.01	0.137 ± 0.06 (0.13 ± 0.02)	29.1 ± 5.30 (0.87 ± 0.02)	0.34 ± 0.02
Hh-mCFP vc (6)	0.418 ± 0.01	0.134 ± 0.03 (0.18 ± 0.04)	44.82 ± 15.0 (0.83 ± 0.04)	0.33 ± 0.01
HhK132D-mCFP (13)	0.40 ± 0.02	0.26 ± 0.09 (0.10 ± 0.03)	28.4 ± 10.4 (0.9 ± 0.02)	0.35 ± 0.02
HhΔCW-mCFP (9)	0.405 ± 0.010	0.21 ± 0.06 (0.1 ± 0.01)	24.4 ± 5.9 (0.9 ± 0.008)	0.34 ± 0.014
HhΔ140-mCFP (7)	0.41 ± 0.01	0.25 ± 0.08 (0.12 ± 0.02)	32.9 ± 8.8 (0.88 ± 0.02)	0.35 ± 0.02
DDPS RNAi (Hh-mCFP diff) (14)	0.416 ± 0.004	0.14 ± 0.03 (0.12 ± 0.03)	50.6 ± 28.7 (0.88 ± 0.03)	0.357 ± 0.014

Average lifetime for GFP and mCFP are 1.9 ± 0.2 ns and 0.80 ± 0.13 ns, respectively (see Table S1). n represents the number of data points from a single experiment. Each experiment was repeated at least twice for all constructs with similar results. Values reported in the table are mean ± the SD. τ_{R1} represents the time scale for the fast-decay component (due to FRET, ns), and τ_{R2} represents decay rate of the slow component (due to rotation of mCFP, ns). A_{R1} and A_{R2} represent amplitude for fast and slow decay, respectively. $r_{0,}$ represents the initial anisotropy value. r_{ss} represents the steady-state anisotropy value obtained from the fit of individual time resolved anisotropy decay.

[a] GFP-GPI-expressing CHO cells depleted of cholesterol (0.03% Saponin, 30 min 0°C) exhibit a single rate of anisotropy decay, corresponding to the rotational correlation time of GFP attached to a membrane linker.

FRET between mCFP molecules compared to Hh-mCFP in the diffuse regions (Figure 6F and Figure S9), confirming that K132 is indeed necessary to keep Hh molecules in close proximity. Furthermore, the decay rates of HhΔ140-mCFP and HhK 132D-mCFP were statistically indistinguishable from mCFP-GPI (Figure S6C; $p > 0.5$; Figure S9). As discussed above, the residual FRET observed in these constructs is likely to be a contribution of the lipid-mediated interactions similar to those observed in the mCFP-GPI molecules (Figure S6A).

Although HhK132D-mCFP is expressed at similar levels at the cell-surface level as Hh-mCFP (Figure S2B), it is unable to form visible clusters (Figures 6D and 6E), analogous to the HhΔ140-mCFP construct (Figures 3D, 3E, 6D, and 6E and Figure S2). Visible clusters are restored when Asp at 132 is replaced by Arg (Figures S7D–S7F), consistent with the hypothesis that an electrostatic interaction between subunits is an evolutionarily conserved feature of Hh. These results suggest that nanoscale clustering by protein sequences in Hh promoted the next level of interactions of the Hh molecule with HSPG moieties to generate visible scale clusters.

Nanoscale Organization Is an Essential Step in Making Hh Competent for Long-Range Signaling

The suboptical organization of Hh demonstrated above appears necessary for its interaction with HSPGs to generate visible clusters at the cell surface. We now probe the functional significance of this level of organization by examining the consequences of its disruption on Hh signaling.

We first confirmed that when expressed in larval tissues, HhK132D-mCFP is lipid modified by assessing its capacity to partition into detergent-phase of the TX-114 phase-partitioning assay (Figure S11). We next tested the signaling efficacy of HhK132D-mCFP in the posterior PM cells of the wing discs (Figures S8A and S8C) and monitored the activation of a target gene, *dpp*-lacZ (Figures S8B and S8C). We find that although HhK132D-mCFP activates *dpp*-lacZ in adjacent anterior PM cells (Figures S8B, S8C, and S10J–S10R), unlike Hh-mCFP (Figures S1A–S1C and S10A–S10C) and Hh-GFP (Figure 1D and Figures S10D–S10F), it fails to activate *dpp*-lacZ expression at a distance in the anterior disc-proper cells. We also use the differential ability of Hh-mCFP isoforms to activate *dpp*-lacZ expression in the PM to provide additional support for the proper lipid modification of HhK132D-mCFP isoform (Figure S12). Although HhK132D-mCFP activates *dpp*-lacZ expression in a restricted fashion, the cholesterol anchor minus isoform activates *dpp*-lacZ expression in the entire anterior domain (HN-mCFP; Figures S12B and S12B′), and the palmitoylation-defective form fails to activate *dpp*-lacZ (HNC85-mCFP; Figures S12C and S12C′). Together with the TX114 phase-partitioning data, the signaling ability and restricted range the HhK132D-mCFP isoform is consistent with its correct lipidation.

To assess the range of Hh signaling mediated by HhK132D-mCFP, we used the Flp-FRT system (Blair, 2003) to express the protein in a small number of disc-proper cells in the anterior compartment. Here, too, it could activate Hh signaling (*dpp*-lacZ expression) in the producing cells and in cells at most one cell diameter away (Figures 7A–7D and 7J). In a similar assay, Hh-GFP was able to turn on *dpp*-lacZ several cell diameters away (Figures 7E–7H and 7J). The lack of activation of the target genes was not due to a low level of protein expression (Figure 7I) or poor signaling efficiency by the mutant protein, because a high threshold target gene, *ptc* (Torroja et al., 2005), is upregulated in the cells expressing HhK132D-mCFP, to the same levels as that observed for Hh-GFP-expressing cells (Figures 7L–7N and

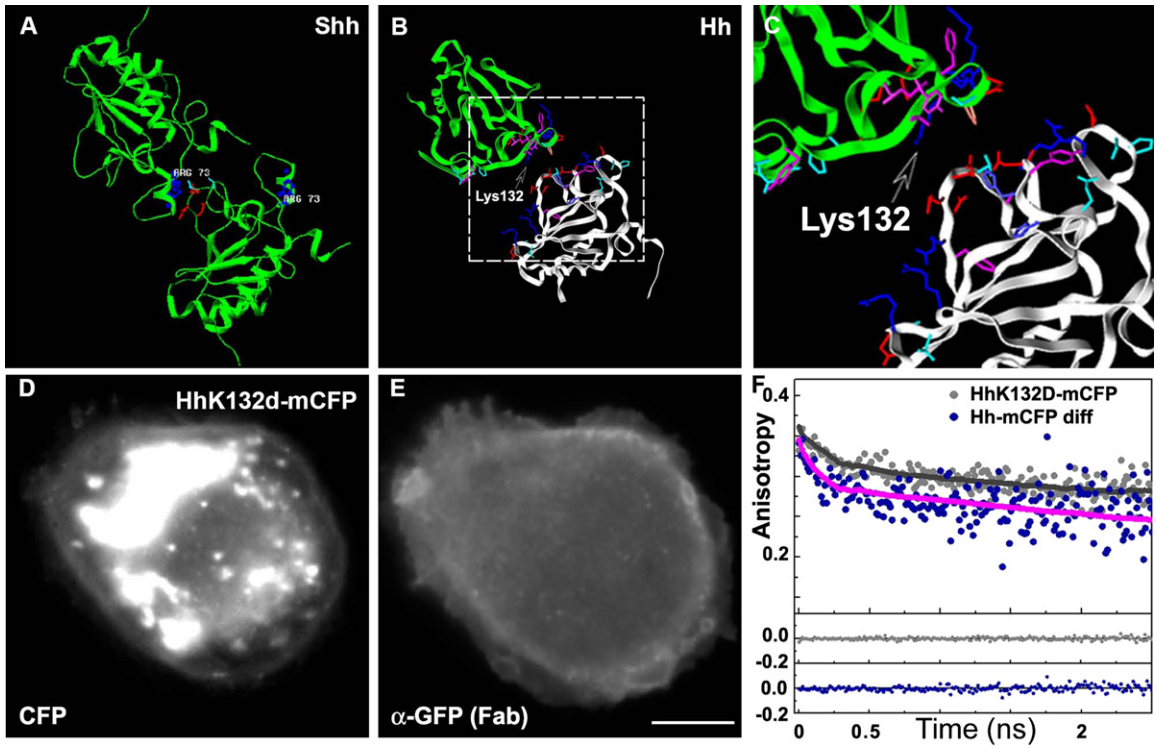

Figure 6. Electrostatic Interaction between Hh Molecules Is Responsible for Nanoscale Proximity

(A) A part of the crystal lattice of Shh (PDB code: 1vhh; [Hall et al., 1995]). Crystal contacts between adjacent molecules are shown for a pair of proteins within the asymmetric unit. Arg73 (in blue; Lys132 is the equivalent residue in Hh) is present in the interface region. Three negatively charged residues (Asp98, Glu99, and Glu100, in red) are present in the loop of the adjacent protomer interface, stabilizing the interaction. Only sidechains of Arg73 and the negatively charged loop in the adjacent molecule are highlighted.

(B and C) Interactions between adjacent molecules as predicted for the *Drosophila* Hh sequence after threading it over the crystal lattice of Shh with MODELER, and Setor for the representation ([B], detail in [C]). Note that Lys132 is also likely to be stabilized by interactions with a negatively charged loop (Asp148-Glu150 and Glu190-Asp191) and that the interface is also predominantly polar. The ratio of polar:hydrophobic at the interface is 21:3 (white chain) and 20:6 (green), involving involve loops 127–131, 146–154, 190–196, 210–213, and 239 of the white chain and loops 114–116, 121–135, 192, 201–202, and 249–253 of the green chain. Side-chain color coding is as follows: pink, hydrophobic residues; cyan, polar residues; red, acidic residues; and blue, basic residues.

(D–F) S2R+ cells transfected with *actin*-GAL4 and UAS-HhK132D-mCFP (D) extracellular pool marked with Cy3α-GFP Fab fragments (E). Independently, anisotropy decay profiles ([F]; gray circles) were obtained from cells expressing HhK132D-mCFP as described in Figure 5 and plotted alongside anisotropy decay profile obtained from Hh-mCFP diff (blue circles). Note that the fast decay rate from HhK132D-mCFP-expressing cells (<0.5 ns region) is detectably slower than the corresponding rate from Hh-mCFP diff (see also Table 1). All decays were fit to a biexponential model and residuals for the fit plotted below. The pink line indicates the fit for data points in blue, and the black line that for data points in gray. The scale bar represents 5 μm.

7K; Figures S8E–S8G). Together, these results imply that the K132D mutation in Hh that abolishes nanoscale and visible scale clustering is signaling competent to adjacent cells and in an autocrine fashion. However, it cannot participate in paracrine signaling (Figure 7J). Transgenic expression of HhK132D-mCFP is also incapable of rescuing the temperature-sensitive lethality exhibited by hh^{ts} flies (data not shown), consistent with the idea that long-range signaling is a necessary function of Hh signaling (Strigini and Cohen, 1997).

DISCUSSION

Visualizing the Organization of Hh

There has been considerable debate regarding the organization and structure of Hh in its functional context. Drawing relationships between biochemically detected forms of Hh (Chen et al., 2004; Gallet et al., 2006; Goetz et al., 2006; Zeng et al., 2001) and levels of organization seen in microscopy of fixed tissues (Gallet et al., 2003), on the one hand, with functional consequences of Hh signaling on the other, have had, perforce, limitations because of the intrinsic nature of methods used. Ideally, a resolution of the relationship between molecular organization and function can come from the examination of all aspects in a context closest to signaling in vivo. Our study establishes conditions for examining Hh organization in live cells at the nano- and visible scale and relates results from these studies directly to the signaling capacity of Hh in the wing discs. This approach identifies novel functions for the Hh protein and demonstrates how molecular organization at hitherto poorly explored nanometer scale relates to important aspects of developmental function.

To visualize Hh organization in living cell membranes, we generated fluorescently tagged Hh homologs (Figures 1A and 3A) by the insertion of a GFP (or mCFP) coding sequence along with

linkers encoding 12 aa residues. Expression of such Hh isoforms in its normal expression domain functionally complements hh^{ts2} allele that is not viable at high temperatures (Figure 1F). Ectopic production of Hh isoforms mimics the effects observed with native Hh protein expression (Figure 1C) (Pallavi and Shashidhara, 2005). In addition, the signaling efficiency of these Hh isoforms is quantitatively similar to that of the native Hh (Figure 1E and Figures S1D–S1I). Thus, this fluorescent Hh analog provides a unique opportunity to interrogate the structure of the functional form of Hh.

Hierarchical Organization of Hh

Our studies clearly show that there are two scales of organization of the lipid-tethered Hh protein: the nanoscale oligomer and the visibly clustered scale (Figures 2, 3B, 3C, and 5A). Although the nanoscale oligomerization is necessary for the generation of the visibly clustered scale (Figures 6D–6F), the mediators of these interactions are located in different parts of the Hh sequence. Nanoscale organization is specified by electrostatic interactions located on the surface of the structured protein domain of the molecule (Figures 6B and 6C), whereas the visibly clustered scale of organization is mediated by the HSPG-interacting CW motif (Figures 4D, 4F, and 4G) in the rather unstructured N terminus of the protein (Rubin et al., 2002). The absence of a clustered distribution in the HhK132D-mCFP and HhΔ140-mCFP isoforms (Figures 3D, 3E, 6D, and 6E) strongly suggests that specific oligomerization of the protein domain presents a dendrimer-like CW motif-containing ligand necessary for interaction with HSPGs at the cell surface. Consistent with this is the observation that oligomers appear to be enriched at the sites where endogenous HSPGs (Dlp) are present in a clustered state (Figures 4A–4C, 4E, and 5A and Figure S5C). On the other hand, the tightly packed organization of the diffusely distributed mCFP in cells expressing the HhΔCW-mCFP isoform (Figure 5B) or in HSPG-depleted cells expressing Hh-mCFP (Figure 5C) provide evidence that interactions with HSPGs are not necessary for the generation of the nanoscale organization. The nanoscale oligomerization appears to be mediated by an electrostatic interaction between subunits, indicated by polar or charged patches in one of the protomers at the predicted interface (Figures 6A–6C) and confirmed in part by mutational studies (Figures 6D–6F). The identification of Lys132 residue at the surface of one of the monomer units and a set of negatively charged residues on the surface of the other monomer unit, by two independent methods, GRAMM docking (Figures S7A and S7B) and a study of stacking interactions in the crystal unit (Figure 6A), supports a key role for this interaction motif as a basis for the formation of the protein-protein interaction surface. Although mutational studies of Lys132 to Asp showing a loss of oligomeric organization at the nanoscale (Figure 6F) and consequently at the visible scale (Figures 6D and 6E) provide evidence for this prediction, the restoration of the visibly clustered organization after converting Asp132 to its vertebrate counterpart, Arg (at position 73 in Shh; Figures S7C and S7D–S7F), further strengthens this argument. The complimentary interaction surface of negatively charged surfaces is not unambiguously identified, since GRAMM docking studies pick out two distinct sites as potential interfaces for energetically favorable docking (Figures 6B and 6C and Figures S7A and S7B). Indeed, the two orientations, one as noticed in the crystal structure packing and another suggested by GRAMM, both involving Lys132 residue at the putative interface, are equivalent in energies (data not shown). This suggests that both orientations and modes of packing between protomers are feasible. Alternately, this could be a reflection of current limitations of "blind" docking algorithms because correct recognition of putative interface for one protein and errors in orientations of the other protein are not uncommon and have been observed (Dunbrack et al., 1997).

Given the different scales available to our analyses, the nanoscale from FRET studies to detect oligomers, and the diffraction-limited optical scale for visualizing the HSPG-mediated clusters, we can correlate the structures that we have identified here with those observed in previous studies by different techniques. The homomeric multimers previously indicated by immunoprecipitation (Zeng et al., 2001) may be understood as representing protein-protein interactions dictated by Lys132 to form native Hh oligomer. The biochemically characterized high molecular weight species (Chen et al., 2004; Gallet et al., 2006; Zeng et al., 2001) are likely to be directly derived from HSPG-containing visibly clustered Hh molecules, which would be expected to be rather resistant to fragmentation during biochemical solubilization procedures. Consistent with this, deletion studies of the CW domain abrogate high molecular weight complexes of Hh (Goetz et al., 2006).

Hh has been shown to form LPS with *Drosophila* embryos (Gallet et al., 2003; Porter et al., 1996). Work done by Callejo et.al. suggests that in wing disc cells, Hh fails to form LPS (Callejo et al., 2006). Consistent with this, we are also unable to unambiguously identify LPS-like particles by using our fixation and cell-surface labeling protocol, in wing disc cells. We believe that the visible clusters of Hh, observed by us at the surface of S2R+ cells and PM cells, have not been reported earlier. It is likely that because embryonic cells and even the disc proper cells of wing discs are very small in size (~3 μm) they fail to provide enough resolution to study cell-surface organization in the plasma membrane of this complex columnar-pseudostratified tissue. Alternatively, as suggested recently (Callejo et al., 2006), LPS are only visualized when cells are permeabilized, and many of these represent endocytic structures. Thus, it is difficult to correlate the scales of organization that we have identified in this study to LPS.

Role of Lipid Modifications

Lipid modifications are likely to play important roles in dictating the mature structure of Hh in the cell membrane; these modifications certainly have an impact on the function of Hh, both in signaling and transport properties of this protein (Chamoun et al., 2001). In this study, however, we have addressed the role of sequence-specific interactions of the protein domain and have therefore compared the cell-surface organization of dually lipidated variants of Hh.

We first analyzed HhΔ140-mCFP, which lacks the entire N-terminal signaling domain except the first 100 residues (Figure 3A′). This protein forms relatively loosely packed structures (characterized in terms of the rate of anisotropy decay and the amplitude of the fast-decay component) that appear

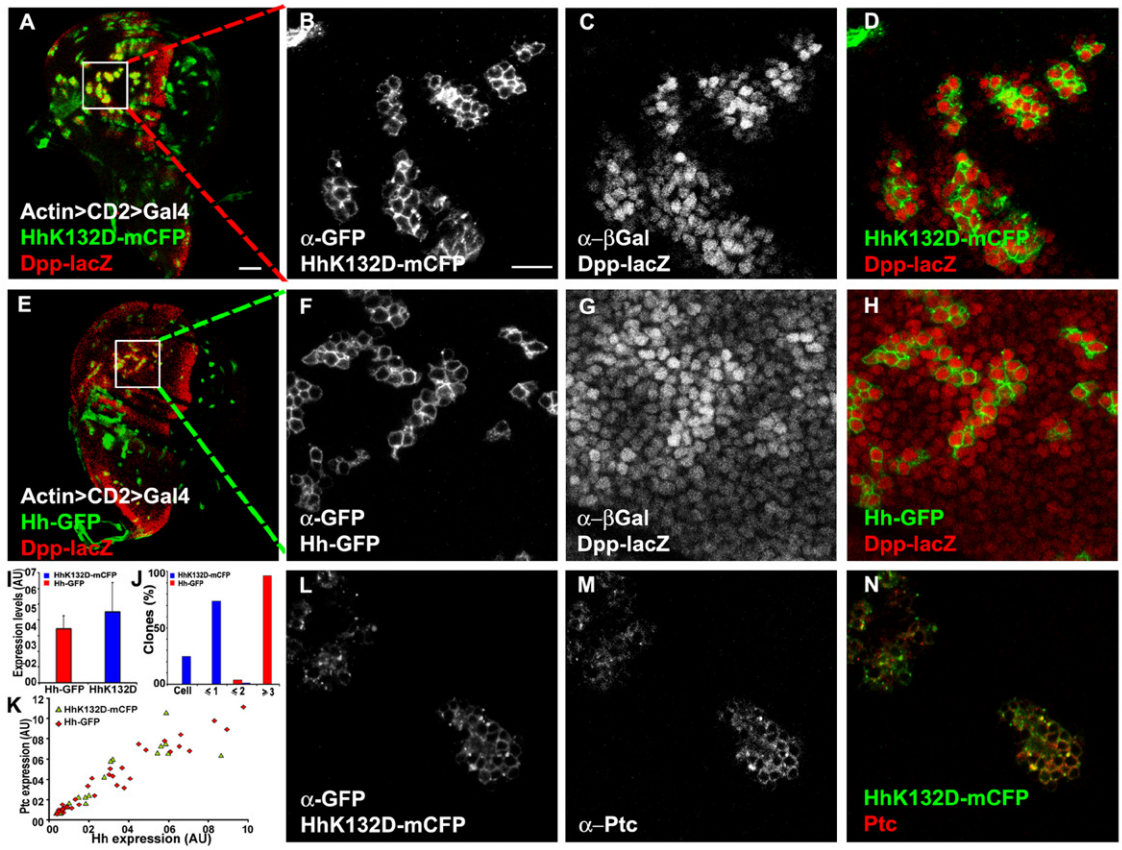
A
Actin>CD2>Gal4
HhK132D-mCFP
Dpp-lacZ
B
α-GFP
HhK132D-mCFP
C
α–βGal
Dpp-lacZ
D
HhK132D-mCFP
Dpp-lacZ
E
Actin>CD2>Gal4
Hh-GFP
Dpp-lacZ
F
α-GFP
Hh-GFP
G
α–βGal
Dpp-lacZ
H
Hh-GFP
Dpp-lacZ
I
HhK132D-mCFP
Hh-GFP
Expression levels (AU)
Hh-GFP HhK132D
J
HhK132D-mCFP
Hh-GFP
Clones (%)
Cell ≤1 ≤2 >3
K
HhK132D-mCFP
Hh-GFP
Ptc expression (AU)
Hh expression (AU)
L
α-GFP
HhK132D-mCFP
M
α–Ptc
N
HhK132D-mCFP
Ptc

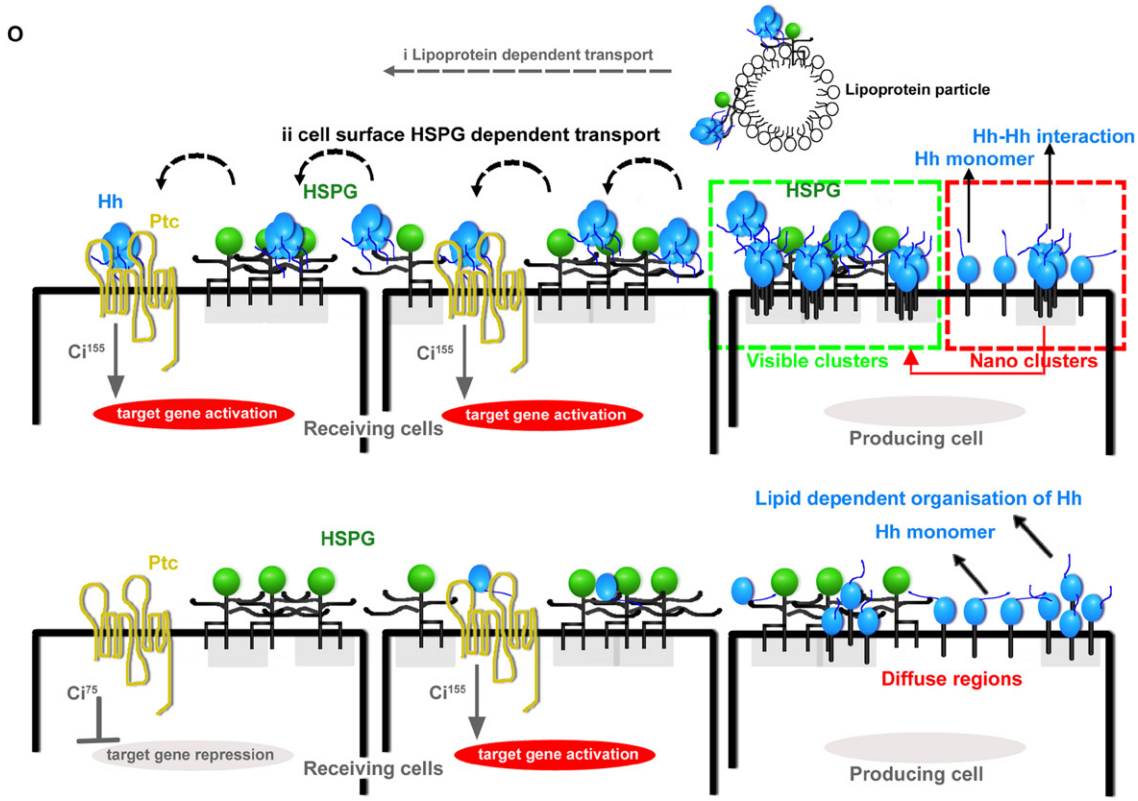
O
i Lipoprotein dependent transport
Lipoprotein particle
ii cell surface HSPG dependent transport
Hh-Hh interaction
Hh monomer
Hh
Ptc
HSPG
HSPG
Ci155
Ci155
target gene activation
target gene activation
Receiving cells
Visible clusters
Nano clusters
Producing cell
Lipid dependent organisation of Hh
Hh monomer
HSPG
Ptc
Ci75
Ci155
target gene repression
target gene activation
Receiving cells
Diffuse regions
Producing cell

remarkably similar to another dually lipidated protein, mCFP-GPI (Figure S6A), which forms small nanoclusters with a large fraction of monomers in membranes of living cells (Sharma et al., 2004). Thus, lipid modifications could provide a template that is loosely preclustered at the nanoscale and provides infrastructure necessary for the densely packed nanoscale organization dictated by the electrostatic interaction surface of protein monomers. Consistent with this hypothesis, the high molecular weight complexes of Hh lacking lipid modifications appear to have a lower stability (Chen et al., 2004; Gallet et al., 2006; Zeng et al., 2001). Preliminary experiments in our laboratory also indicate that the configuration of the oligomeric species is significantly disrupted in variants lacking one or both lipid anchors (N.V. and D.G., unpublished data). Thus, in addition to a role in Hh signaling, lipid modifications could influence the nature of higher-order species. However, as noted earlier (Figures 3D, 3E, and 5D and Figure S6), the mere presence of lipid modifications is not sufficient to provide an explanation for the distinct scales of structures observed for the Hh protein.

Functional Consequences of Hierarchical Organization

The results presented here allow a functional dissection of the organization of Hh into two parts: the dually lipidated structure as a fundamental signaling unit, and higher-order, tightly packed oligomers as competent for interacting with HSPG-containing molecules. Structural insight into this segregation of function comes from analysis of the interface between two monomers. Although, as indicated above, the precise location of the negatively charged surface that interacts with Lys 132 at the monomer-monomer interface has not been identified, the interface appears to be largely represented by a set of clustered polar or charged residues (Figures S7A and S7B) that are characteristic of many multimeric interactions, wherein the monomer is capable of existing as an independent unit (De et al., 2005). This suggests that the monomer is fully competent to carry out its basic function (signaling) and that higher-order arrangements provide additional functionality (binding HSPGs). Indeed, data obtained with the HhK132D isoform, capable of efficient autocrine signaling via the canonical Hh signaling pathway and activation of high-threshold target genes (Figures 7A–7D, 7L–7N, and 7K; Figures S8E–S8G), appears to bear out this contention. This mutant Hh protein is also likely to serve as a tool to distinguish the role of long-range signaling due to secretion of Hh or via direct access of membrane-tethered Hh proteins.

As suggested above, nanoscale oligomerization provides the multivalency necessary for Hh to interact with HSPGs, in turn allowing it to form visible clusters. Recently, it has been shown that lipid-modified Hh can be released from the plasma membrane on lipoprotein particles for long-range signaling (Panakova et al., 2005). Hh trafficking and signaling also depend on HSPGs (Lin, 2004), in particular the glypicans (Han et al., 2004). In addition, lipoprotein particles have been shown to contain glypicans (Eugster et al., 2007). Thus, oligomerization of Hh would be essential for interaction with HSPGs present on the cell surface or on lipoprotein particles and thereby effect long-range signaling. Conversely, prevention of oligomerization should prevent association with HSPGs, and consequently long-range signaling. The results obtained here, in the context of the restricted signaling range of the HhK132D isoform (Figure 7; Figures S8A–S8C and S10J–S10R) strongly implicate an interaction with HSPGs as a vehicle for facilitating transport of Hh. In HSPG-depleted context, signaling is observed in Hh-producing clones, as expected, but interestingly, only low-affinity targets are activated (Callejo et al., 2006). This is different from the nature of signaling in HhK132D mutant-expressing clones, where even high target genes (Ptc) are upregulated (Figures 7K and 7L–7N and Figures S8E–S8G). Thus, HSPGs are likely to have at least two distinct roles with respect to Hh signaling: They are involved in the transport of Hh for long-range signaling (Bellaiche et al., 1998; Callejo et al., 2006; Han et al., 2004) but additionally may function in the modulation of the extent of Hh activity by interacting with other components of the pathway, such as, perhaps, Ptc and Smo. The singular "disability" of the HhK132D mutant uncovers this "other" role of HSPGs, whereas in HSPG-depleted cells, both roles of Hh are affected.

Although these results demonstrate an essential function for nanoscale organization, we would like to test whether abolition

Figure 7. Functional Significance of Hierarchical Organization of Hh

(A–H) Confocal image and magnified insets ([B]–[D] and [F]–[H]) of a wing disc with flp-out clones expressing HhK132D-mCFP (A–D) or Hh-GFP (E–H), generated as described in the Supplemental Experimental Procedures, and stained for Hh variants (anti-GFP in [B] and [F]; green in [A], [E], [D], and [H]) and Dpp expression (β-Gal in [C] and [G]; red in [A], [E], [D] and [H]). Note ectopic activation of *dpp*-lacZ by cells expressing HhK132D-mCFP and only in adjacent cells, whereas cells expressing Hh-GFP activate *dpp*-lacZ several cell diameters away from the expressing cells.

(I) Expression levels (red bar for Hh-GFP and blue bar for HhK132D) are plotted as mean ± SD. Images are acquired with identical acquisition parameters.

(J) Histogram shows the fraction of clones obtained that activate *dpp*-lacZ only within the clone (Cell) or one (<1), two (<2), or more (>3) cell diameters away. Approximately 80 clones were examined in two independent experiments.

(K) Graph compares signaling efficiency (anti-Ptc-levels) at diffferent HhK132D-mCFP (green triangles) and Hh-GFP (red rhomboids) expression levels in clones as described in the Supplemental Experimental Procedures. Surface levels of Hh-GFP and HhK132D-mCFP (anti-Hh) in flp-out clones are plotted along the x axis; autonomous activation of Ptc levels (anti-Ptc-binding in corresponding areas) is represented along the y axis (see images in Figures S1G–S1I and S8E–S8G).

(L–N) Single-color (L and M) and merged (N) confocal images of flp-out clones expressing HhK132D-mCFP (α-GFP, L; green in [N]) activate a higher threshold target gene, Ptc (anti-Ptc, M; red in [N]) in autocrine fashion.

(O) Model representing the surface organization, transport, and signaling capacity of Hh (top) and HhK132D isoforms (bottom). Nanoscale Hh oligomers (blue) in the diffuse regions of the cell membrane (red box) are selectively enriched in visible clusters (green box) along with cell-surface HSPGs containing glypicans (multiply branched structures, green). Upon release from producing cells, these Hh oligomers may be transported across several cell diameters either via interaction with cell-surface HSPGs (black broken arrows) and/or by HSPGs incorporated in lipoprotein particles (gray broken arrow). HhK132D fails to form compact nanoscale oligomers and thus unable to interact efficiently with cell-surface HSPGs, resulting in failure of long-range transport. Signaling capacity is indicated by the ability of the Hh variants to turn on target genes in the receiving cells. Autocrine signaling capacity for both variants is similar. Scale bars represent 40 (A–C) and 10 (B–D, F–H, and L–N) μm.

of the ability to interact with HSPGs, and thereby visible clustering but not nanoscale organization, could also mimic the same results. The HhΔCW mutant offers an opportunity for just such a test. Unfortunately, the HhΔCW-mCFP, although expressed normally in the anterior compartment of the discs or in the PM of wing discs, is incapable of signaling via the Hh signaling pathway even in an autocrine manner (data not shown). One possibility is that the deleted CW domain contains sites required for activating Hh signaling through interactions with Ptc.

Conclusion

A precisely calibrated, long-range signaling potential is the hallmark of a secreted morphogen such as Hh. This requires specific mechanisms for its production, transport across cell layers, and reception. The work described here shows that Hh is hierarchically organized via critical cues present in the sequence of the molecule and that different scales of organization need to be examined to unravel the mechanisms of signaling and transport of this evolutionarily conserved morphogen (Figure 7O). Hh forms nanoscale oligomers because of electrostatic interactions between evolutionarily conserved amino acid residues present at potential monomer-monomer interaction interfaces. Although oligomerization specifies an interaction with HSPGs necessary for the transport of Hh across many cell diameters, the monomer is independently capable of locally activating Hh signaling pathways.

EXPERIMENTAL PROCEDURES

Materials and details of additional methods are given in Supplemental Data available online.

Homology Modeling Hh and Docking Studies

The N-terminal domain of Hh of *Drosophila melanogaster* (HhDM; Swissprot [Bairoch and Apweiler, 1996]) was modeled with the crystal structure coordinates of the N-terminal domain of Shh (Hall et al., 1995) available in Protein Data Bank (Berman et al., 2000) as a template as described in the Supplemental Data.

The energy minimized homology model of HhDM was supplied twice to GRAMM (GRAMM, V1.03) in order to generate various possible modes of homodimer formation with a grid size of 2.1Å. One hundred docked models were generated and checked for favorable interactions.

Time-Resolved Anisotropy Measurements

For the measurement of the nanoscale organization of Hh variants, S2R+ cells transfected with Hh-GFP or Hh-mCFP variants were mounted. TRA measurements were made as described (Altman et al., 2007), with 63× 1.45 NA Apochromat (Zeiss), and 850 nm (CFP) and 920 nm (GFP) excitation wavelengths of the femtosecond pulsed Ti-Saffire Laser (Spectra Phys). All emission photons were directed toward the nondescanned detectors through a 680 nm reflector (Zeiss). The laser beam was parked at the center of the field. Visible clusters and diffuse regions were manually selected with fast multiphoton scanning and brought to the center of the field prior to collection of the data. The data were fit to multiexponential fits as described (Figure S4 and Altman et al., 2007). p values obtained from an unpaired Student's t test were used to make statistical comparisons between different measurements.

Multiphoton excitation results in confocal excitation at a single point on the specimen, unlike a single-photon excitation, where photons from the entire cell volume may be collected (Altman et al., 2007). Multiphoton excitation coupled with the ability to locate the confocal excitation volume near the edge of the cell where the contribution of the internal pools is negligible allows fair analysis of TRA from cell-surface pool. We deliberately focused on the intracellular pool for the TRA measurements and found that the rate of TRA decay is faster in the intracellular structures (Figure S13). Thus, if after all precautions there is still some contribution from the intracellular proteins, this will result in overestimation of the extent of FRET in case of mutants, and not an underestimation. Credible TRA measurements of the intracellular pool of Hh-GFP or mCFP are not possible because this pool is very small.

Extracelluar Staining

Surface pool of the Hh variants was marked with Cy5- or A568-labeled Fab fragments of anti-GFP (mouse, Bangalore Genei) by incubation of live cells on ice for 30 min. Cells are then washed with M1 and imaged live, unless otherwise mentioned.

For extracellular staining of peripodial membrane cells of wing imaginal disc, larvae of the required genotype were dissected, and disc preparations were incubated with 2–4 μg/ml labeled Fab fragments one ice for 20 min in a 1.5 ml centrifuge tube. For removal of the unbound antibodies, discs are washed twice with prechilled 1× PBS, fixed with 4% paraformaldehyde for 20 min, and imaged.

Depletion of Endogenous HSPGs

S2R+ cells were incubated in growth medium supplemented with double-stranded RNA (dsRNA) against all the four HSPGs, namely-Dally, Dlp, Perlecan, and Syndecan (DDPS), or dsRNA against Dally and Dlp (DD). Cells were resuspended in fresh medium supplemented with dsRNA after 6 days. After 12 days of incubation in dsRNA-containing medium, cells were incubated with transfection mix containing UAS Hh-mCFP and *actin*-GAL4 cDNA and dsRNA for 3 days. Cells were than plated in coverslip bottom dishes and used for different assays. Endogenous Dlp levels were examined by immunostaining with mouse anti-Dlp (mouse, supernatant, DSHB).

Microscopy and Image Processing

High-resolution wide-field images were collected with a Nikon TE 300 inverted microscope. Images were analyzed with Metamorph software (Universal Imaging, PA) as described earlier (Sharma et al., 2004). A laser scanning confocal microscope (Olympus FV1000) was used for confocal fluorescence imaging with appropriate factory set filters and dichroics. Images were analyzed with FV10-ASW 1.4 software.

SUPPLEMENTAL DATA

Supplemental Data include Supplemental Experimental Procedures, thirteen figures, Supplemental References, and one table and can be found with this article online at http://www.cell.com/cgi/content/full/133/7/1214/DC1/.

ACKNOWLEDGMENTS

We would like to thank P. Ingham (Institute of Molecular and Cell Biology, Singapore) for UAS Ptc-YFP stock; T. Kornberg (University of California, San Francisco), P. Therond (Institute of Signaling, Developmental Biology, and Cancer Research, France), and S. Eaton (Max Planck Institute of Molecular Cell Biology and Genetics, Dresden, Germany) for anti-Hh antibodies; N. Periasami (Tata Institute of Fundamental Research, Mumbai) for his guidance for the analysis of TRA measurements; and H. Krishnamurthy at the National Centre for Biological Sciences Central Imaging and Flow Facility for help with the multiphoton system. S.M. and N.V. acknowledge grants from the Human Frontier Science Program (RGP0050/2005-C) and Swarnajayanti Fellowship from the Department of Science and Technology, Government of India, and K.V. from Department of Biotechnology, Government of India, for generous support. We gratefully acknowledge S. Ramaswamy (University of Iowa) for insights into the crystal structure of Shh, V. Rodrigues for helpful suggestions on the manuscript, K.G. Guruharsha, and the Mayor and Shashidhara laboratories for their help.

Received: September 13, 2007
Revised: February 15, 2008
Accepted: May 8, 2008
Published: June 26, 2008

REFERENCES

Altman, D., Goswami, D., Hasson, T., Spudich, J.A., and Mayor, S. (2007). Precise positioning of myosin VI on endocytic vesicles in vivo. PLoS Biol. *5*, e210.

Ashe, H.L., and Briscoe, J. (2006). The interpretation of morphogen gradients. Development *133*, 385–394.

Bairoch, A., and Apweiler, R. (1996). The SWISS-PROT protein sequence data bank and its new supplement TREMBL. Nucleic Acids Res. *24*, 21–25.

Bellaiche, Y., The, I., and Perrimon, N. (1998). Tout-velu is a Drosophila homologue of the putative tumour suppressor EXT-1 and is needed for Hh diffusion. Nature *394*, 85–88.

Berman, H.M., Bhat, T.N., Bourne, P.E., Feng, Z., Gilliland, G., Weissig, H., and Westbrook, J. (2000). The Protein Data Bank and the challenge of structural genomics. Nat. Struct. Biol. Suppl. *7*, 957–959.

Blair, S.S. (2003). Genetic mosaic techniques for studying Drosophila development. Development *130*, 5065–5072.

Callejo, A., Torroja, C., Quijada, L., and Guerrero, I. (2006). Hedgehog lipid modifications are required for Hedgehog stabilization in the extracellular matrix. Development *133*, 471–483.

Chamoun, Z., Mann, R.K., Nellen, D., von Kessler, D.P., Bellotto, M., Beachy, P.A., and Basler, K. (2001). Skinny hedgehog, an acyltransferase required for palmitoylation and activity of the hedgehog signal. Science *293*, 2080–2084.

Chen, M.H., Li, Y.J., Kawakami, T., Xu, S.M., and Chuang, P.T. (2004). Palmitoylation is required for the production of a soluble multimeric Hedgehog protein complex and long-range signaling in vertebrates. Genes Dev. *18*, 641–659.

DasGupta, R., Kaykas, A., Moon, R.T., and Perrimon, N. (2005). Functional genomic analysis of the Wnt-wingless signaling pathway. Science *308*, 826–833.

De, S., Krishnadev, O., Srinivasan, N., and Rekha, N. (2005). Interaction preferences across protein-protein interfaces of obligatory and non-obligatory components are different. BMC Struct. Biol. *5*, 15.

Dunbrack, R.L., Jr., Gerloff, D.L., Bower, M., Chen, X., Lichtarge, O., and Cohen, F.E. (1997). Meeting review: The second meeting on the critical assessment of techniques for protein structure prediction (CASP2), Asilomar, California, December 13–16, 1996. Fold. Des. *2*, R27–R42.

Eugster, C., Panakova, D., Mahmoud, A., and Eaton, S. (2007). Lipoprotein-heparan sulfate interactions in the Hh pathway. Dev. Cell *13*, 57–71.

Gallet, A., Rodriguez, R., Ruel, L., and Therond, P.P. (2003). Cholesterol modification of hedgehog is required for trafficking and movement, revealing an asymmetric cellular response to hedgehog. Dev. Cell *4*, 191–204.

Gallet, A., Ruel, L., Staccini-Lavenant, L., and Therond, P.P. (2006). Cholesterol modification is necessary for controlled planar long-range activity of Hedgehog in Drosophila epithelia. Development *133*, 407–418.

Gautier, I., Tramier, M., Durieux, C., Coppey, J., Pansu, R.B., Nicolas, J.C., Kemnitz, K., and Coppey-Moisan, M. (2001). Homo-FRET microscopy in living cells to measure monomer-dimer transition of GFP-tagged proteins. Biophys. J. *80*, 3000–3008.

Goetz, J.A., Singh, S., Suber, L.M., Kull, F.J., and Robbins, D.J. (2006). A highly conserved amino-terminal region of sonic hedgehog is required for the formation of its freely diffusible multimeric form. J. Biol. Chem. *281*, 4087–4093.

Hall, T.M., Porter, J.A., Beachy, P.A., and Leahy, D.J. (1995). A potential catalytic site revealed by the 1.7-A crystal structure of the amino-terminal signalling domain of Sonic hedgehog. Nature *378*, 212–216.

Han, C., Belenkaya, T.Y., Wang, B., and Lin, X. (2004). Drosophila glypicans control the cell-to-cell movement of Hedgehog by a dynamin-independent process. Development *131*, 601–611.

Lin, X. (2004). Functions of heparan sulfate proteoglycans in cell signaling during development. Development *131*, 6009–6021.

Lu, X., Liu, S., and Kornberg, T.B. (2006). The C-terminal tail of the Hedgehog receptor Patched regulates both localization and turnover. Genes Dev. *20*, 2539–2551.

Lum, L., Zhang, C., Oh, S., Mann, R.K., von Kessler, D.P., Taipale, J., Weis-Garcia, F., Gong, R., Wang, B., and Beachy, P.A. (2003). Hedgehog signal transduction via Smoothened association with a cytoplasmic complex scaffolded by the atypical kinesin, Costal-2. Mol. Cell *12*, 1261–1274.

Mann, R.K., and Beachy, P.A. (2004). Novel lipid modifications of secreted protein signals. Annu. Rev. Biochem. *73*, 891–923.

Mayor, S., and Maxfield, F.R. (1995). Insolubility and redistribution of GPI-anchored proteins at the cell surface after detergent treatment. Mol. Biol. Cell *6*, 929–944.

Pallavi, S.K., and Shashidhara, L.S. (2005). Signaling interactions between squamous and columnar epithelia of the Drosophila wing disc. J. Cell Sci. *118*, 3363–3370.

Panakova, D., Sprong, H., Marois, E., Thiele, C., and Eaton, S. (2005). Lipoprotein particles are required for Hedgehog and Wingless signalling. Nature *435*, 58–65.

Pepinsky, R.B., Zeng, C., Wen, D., Rayhorn, P., Baker, D.P., Williams, K.P., Bixler, S.A., Ambrose, C.M., Garber, E.A., Miatkowski, K., et al. (1998). Identification of a palmitic acid-modified form of human Sonic hedgehog. J. Biol. Chem. *273*, 14037–14045.

Phelps, C.B., and Brand, A.H. (1998). Ectopic gene expression in Drosophila using GAL4 system. Methods *14*, 367–379.

Porter, J.A., von Kessler, D.P., Ekker, S.C., Young, K.E., Lee, J.J., Moses, K., and Beachy, P.A. (1995). The product of hedgehog autoproteolytic cleavage active in local and long-range signalling. Nature *374*, 363–366.

Porter, J.A., Ekker, S.C., Park, W.J., von Kessler, D.P., Young, K.E., Chen, C.H., Ma, Y., Woods, A.S., Cotter, R.J., Koonin, E.V., and Beachy, P.A. (1996). Hedgehog patterning activity: Role of a lipophilic modification mediated by the carboxy-terminal autoprocessing domain. Cell *86*, 21–34.

Rao, M., and Mayor, S. (2005). Use of Forster's resonance energy transfer microscopy to study lipid rafts. Biochim. Biophys. Acta *1746*, 221–233.

Rubin, J.B., Choi, Y., and Segal, R.A. (2002). Cerebellar proteoglycans regulate sonic hedgehog responses during development. Development *129*, 2223–2232.

Sharma, P., Varma, R., Sarasij, R.C., Ira, Gousset, K., Krishnamoorthy, G., Rao, M., and Mayor, S. (2004). Nanoscale organization of multiple GPI-anchored proteins in living cell membranes. Cell *116*, 577–589.

Strigini, M., and Cohen, S.M. (1997). A Hedgehog activity gradient contributes to AP axial patterning of the Drosophila wing. Development *124*, 4697–4705.

Tabata, T., and Takei, Y. (2004). Morphogens, their identification and regulation. Development *131*, 703–712.

Torroja, C., Gorfinkiel, N., and Guerrero, I. (2005). Mechanisms of Hedgehog gradient formation and interpretation. J. Neurobiol. *64*, 334–356.

Varma, R., and Mayor, S. (1998). GPI-anchored proteins are organized in submicron domains at the cell surface. Nature *394*, 798–801.

Zeng, X., Goetz, J.A., Suber, L.M., Scott, W.J., Jr., Schreiner, C.M., and Robbins, D.J. (2001). A freely diffusible form of Sonic hedgehog mediates long-range signalling. Nature *411*, 716–720.

Zhang, J., Campbell, R.E., Ting, A.Y., and Tsien, R.Y. (2002). Creating new fluorescent probes for cell biology. Nat. Rev. Mol. Cell Biol. *3*, 906–918.